MS-No.: egusphere-2024-2495

Title: Urban Area Observing System (UAOS) Simulation Experiment Using DQ-1 Total Column Concentration Observations

Authors: Jinchun Yi, Yiyang Huang, Zhipeng Pei, Ge Han

Item-by-item reply to Anonymous Referee #1

September 24, 2024

Dear reviewers:

Thank you very much for reviewing our manuscript and providing valuable feedback. We sincerely appreciate your patience and detailed comments. Under your guidance, we have carefully addressed each of your comments and made corresponding revisions and additions. All your words are in black and our item-to-item responses are in blue. We have included our revisions for some comments directly for your convenience.

****

General comments:

The manuscript uses innovative active remote sensing CO2 data from the actual Chinese DQ-1 lidar satellite mission and shows the potential of the XCO2 IPDA lidar onboard DQ-1 to assess anthropogenic CO2 fluxes from megacities. The WRF-STILT model is used to assess atmospheric transport, and the ODIAC inventory provides emission estimates which are scaled to the observations using a regional inverse modelling approach. The authors additionally present a case study attempting at separating natural and anthropogenic CO2 emissions around Beijing, and investigate uncertainties due to measurement (XCO2) and model errors (wind speed and direction).

The data treatment and modelling approach is appropriate, but I am missing more details on how the background CO2 level is determined in the lidar measurements, which, in my experience, is a crucial issue. All major points are well presented, yet some statements, particularly those concerning the natural emissions, are based on the examination of very few cases, and thus need to be re-formulated more cautiously. It would be helpful to include more megacity overpasses to consolidate the statements. Some figures have to be improved. The basic approach, the selection of two cities and the design of several figures is adopted from Ye et al (JGR-A 2020), so they should be more amply cited. The manuscript covers an important topic addressed with novel instrumentation and is a good match to ACP (or AMT). I therefore recommend accepting the manuscript, but only after my recommendations and comments have been addressed.

ANSWER: Thank you for your positive comments. We really appreciate your encouragement and support. To facilitate the readers' understanding of this study, we have carefully revised the whole manuscript according to your comments.

Mandatory changes:

1.Section 2.3.3 Background XCO2: own experience tells me that determining the background XCO2 level is the most critical part of data treatment. Please be more precise in the description of your DWT approach. Use the example of Fig 6b where I find the background gradient so strong that its determination must be particularly challenging. Add one or more plots to illustrate how the DWT works. Did you test other thresholds (line 247)? Why did you select mean + 0.5 sigma(XCO2) as threshold?

ANSWER: To derive $ffXCO2$, which represents the enhancement of $XCO2$ attributed to fossil fuel emissions, we need to subtract the background $XCO2$ from the observational data obtained by DQ-1(Ye et al., 2020). In the study by Ye et al. (JGR-A, 2020), XCO2 is decomposed into two components: $XCO2_{trend}$ and $XCO2_{local}$. Here, $XCO2_{trend}$ represents the non-local trend, while the standard deviation σ_{local} of $XCO2_{local}$ indicates variations at the local scale. We filtered the XCO2 samples with $XCO2 < XCO2_{trend} + 0.5\sigma_{local}$ (the choice of $0.5\sigma_{local}$ as the threshold is mentioned here, and we conducted experiments with different thresholds. Given the similarity of our study area to that of Ye et al. (JGR-A 2022), we adopted her selected threshold for our experiments.) These filtered data are designated as "background samples" (represented by blue triangles in Figures 3, 4, 6, and 8) due to their lower spatial variability at the local scale compared to samples affected by urban ffCO2 emissions. We then performed linear regression based on the "background samples" to recalculate the linear regression line, referred to as the "background line." This "background line" method accounts for spatial trends in the background data. Unlike Ye et al. (JGR-A 2022), we utilized the low-frequency (approximate) coefficients obtained from DWT to characterize

The Discrete Wavelet Transform (DWT) is an approximate wavelet transformation method that decomposes a signal into approximation coefficients and detail coefficients at different scales. DWT employs discrete wavelet functions and discrete time scales, achieving signal decomposition through filtering and downsampling operations(Alessio et al., 2016).Typically, DWT decomposes a signal into a set of high-frequency and low-frequency sub-signals. Through successive decomposition, the discrete wavelet transform divides the data into different frequency bands. These frequency bands are generated by a series of wavelet and scaling functions, enabling the capture of both detailed and trend information within the data(Lang et al., 1995).

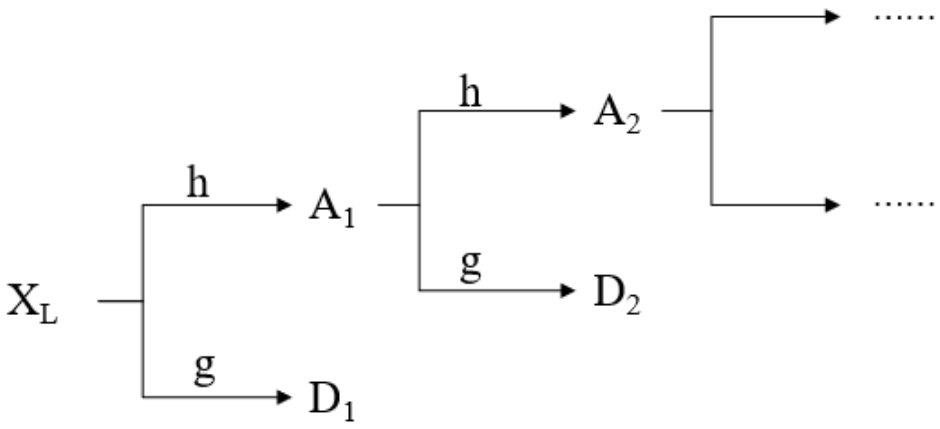

Figure S1. Schematic diagram of the principle of discrete wavelet transform

Figure S1 illustrates the working principle of the Discrete Wavelet Transform (DWT). For a signal XL of length L (representing the single-track DQ-1 XCO2 pseudo-data in this study), the wavelet transform (equivalent to a bandpass filter) decomposes it into high-pass coefficients D1and approximation coefficients A1 (where the detail component D1 corresponds to filtering with a high-pass filter, and the approximation component A1 corresponds to filtering with a low-pass filter). The approximation coefficients are then further decomposed into relatively high-pass coefficients D2 and approximation coefficients A2, and this process continues iteratively. Figure S1 displays only two levels of wavelet decomposition. The equation for the first-level decomposition of DWT is as follows:

$$A_1(L) = \sum_k X_L(k) * h(k-L) \quad 1$$

$$D_1(L) = \sum_k X_L(k) * g(k-L) \quad 2$$

Where $A_1(L)$ represents the low-frequency (approximation) coefficients, and $D_1(L)$ denotes the high-frequency (detail) coefficients. $h(k)$ and $g(k)$ are the coefficients of the low-pass and high-pass wavelet filters, respectively. $X_L(k)$ is the initial input signal, and the input signal for the n-th level wavelet transform is A_{n-1}. We appreciate your inquiry regarding the background gradient in Figure 6b of the manuscript. Next, we will illustrate how to determine the background line using DWT and linear regression, using the track of DQ-1 passing over Beijing on December 1, 2022, as an example.

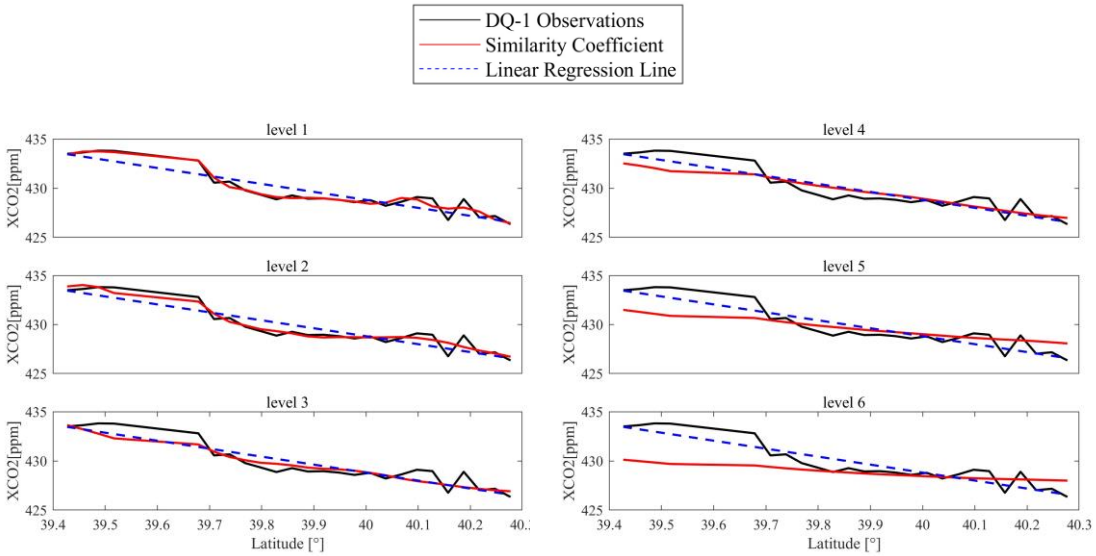

Figure S2. Level 1-6 wavelet transform applied to $XCO2_{trend}$ (red line in figure) derived from DQ-1 orbital pseudo-data (black line in figure) and $XCO2_{trend}$ derived from linear regression (blue dashed line in figure) for the DQ-1 orbital pseudo-data (black line in figure) transiting Beijing on 01 December 2022

Figure S2 displays the extracted $XCO2_{trend}$ from the 1st to the 6th levels of wavelet decomposition (shown as the red lines). The blue dashed lines in S2 represent the $XCO2_{trend}$ obtained using the linear regression method from the background line extraction approach of Ye et al. (JGR-A 2022). As the number of wavelet decomposition levels increases, the extracted $XCO2_{trend}$ becomes smoother and more horizontal, with decreasing gradient changes with latitude. Therefore, selecting an appropriate decomposition level based on different tracks is essential. It can be observed that the $XCO2_{trend}$ derived from the first and second levels of wavelet decomposition closely follows the trend of the pseudo-data along the track, failing to adequately filter out high-frequency information. In contrast, the $XCO2_{trend}$ from the third and fourth levels aligns more closely with the background line derived from linear regression, while the results from the fifth and sixth levels gradually approach horizontal, which does not conform to the desired background line that incorporates latitude gradients.

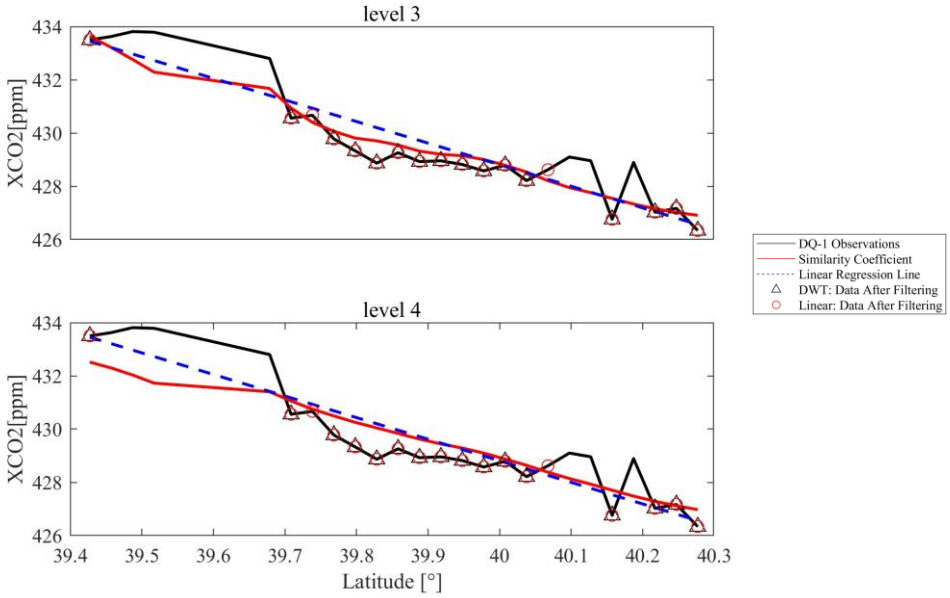

Figure S3. Pseudo-data points involved in the computation of the background line (black hollow triangles in the figure) screened using the third- and fourth-level wavelet transforms, respectively, and background points (red hollow circles) screened using linear regression. The black, red line and blue dashed line are the same as defined in Figure S2.

Figure S3 illustrates the $XCO2_{trend}$ extracted using the third and fourth levels of wavelet decomposition (red lines) from the DQ-1 pseudo-data passing over Beijing on December 1, 2022, along with the data points used for background line calculations (black hollow triangles). Additionally, it includes the $XCO2_{trend}$ extracted using the method of Ye et al. (JGR-A 2022) (blue dashed lines) and the corresponding data points for background line calculations (red hollow circles). In this scenario, the data points used for calculating the background line from the third and fourth wavelet levels are identical. However, the linear regression method filters out two more data points (39.7389° N and 40.0677° N) compared to the DWT approach.

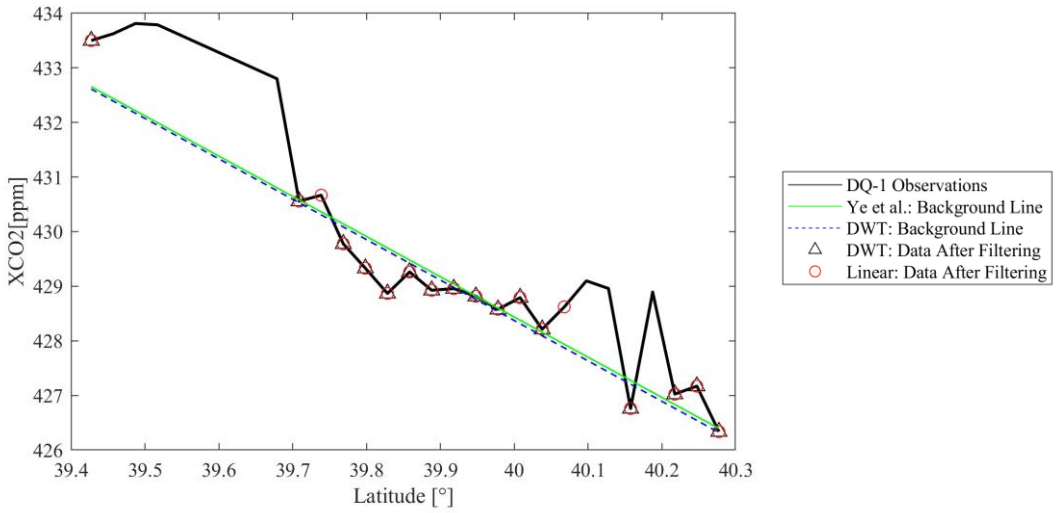

Figure S4. Background line derived using DWT (blue dashed line) and background line derived from linear regression (green line). The black line represents pseudo-observations from DQ-1, the black hollow triangles are background points filtered using DWT, and the red hollow circles are background points filtered by linear regression.

Figure S4 presents the background lines derived from the DQ-1 pseudo-data passing over Beijing on December 1, 2022, using the DWT method (blue dashed line) and the method from Ye et al. (JGR-A 2022) (green line). It is evident that although there is a difference of two data points in the selection of background data for calculations using these two methods, the extracted background lines are essentially indistinguishable.

2.Figure 3: It is unclear where the CO2 maxima in panels a and b come from, given that panels c and d show complex wind situations. Please add the column averaged footprint figures (like fig 2c) to clarify this. Could the maximum at 24.2 N in panel a come from another source in the southeast? The easterly winds suggest this. Please explain. Panels c and d are too small to see the colored DQ-1 XCO2 data, only the orbits are visible. Explain in the caption the blue triangles.

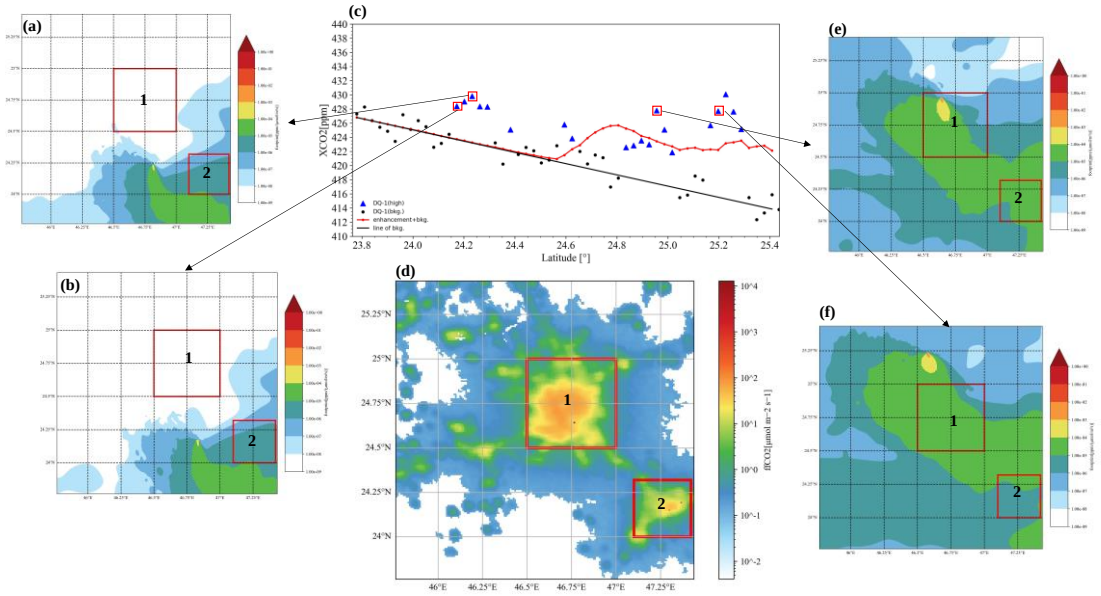

Figure S5. Shows the XSTILT (a, b, e, f) at the location of the partially apparent XCO2 enhancement in the orbit in Fig. 3a of the manuscript. Panel c is Figure 3a from the manuscript and panel d represents the fossil fuel emission inventory now of orbital transit. The main emission sources in the urban area are boxed in red.

ANSWER: Thank you very much for your insightful questions and suggestions regarding Figure 3 in the manuscript. Figure S5 illustrates the enhanced XSTILT data from the orbital data passing over Riyadh on March 2, 2023 (Figure S5c corresponds to Figure 3a in the manuscript), with panels S5a, b, e, and f showing specific enhancements. Panel S5d displays the ODIAC fossil fuel emissions inventory for this track, with two red boxes indicating the locations of major emissions sources (which correspond to the same latitude and longitude ranges as the red boxes in panels S5a, b, e, and f). Panels a and b show that the DQ-1 observational data recorded significant enhancements in XCO2, which were not captured by the simulation results. You mentioned in your suggestions whether the peak at 24.2°N in Figure 3a might originate from another source in the southeast. The easterly winds seem to support this possibility. In our study area, the southeastern source comes from red box 2, and the footprint observed in panels a and b at this location is less than 1e-05. Therefore, it can be concluded that the source in region 2 has a minimal impact on the enhancement of XCO2. The observed XCO2 enhancement from DQ-1 may be influenced by sources located outside the southeastern boundary of the study area. In panels e and f, it can be seen that the observed XCO2 enhancements at these two locations are consistent with the simulated XCO2 enhancements, primarily influenced by source 1 (red box 1).

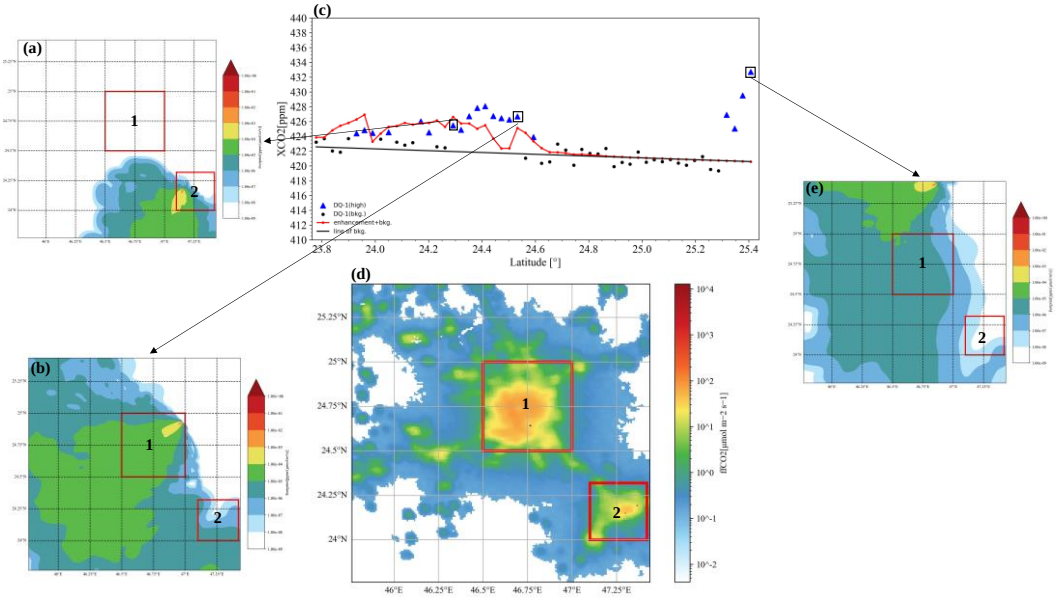

Figure S6. Like Fig. S5, the XSTILT for the case of Fig. 3b in the manuscript is shown (a, b, e).

Panels a and b illustrate the XCO2 enhancements simulated from sources 1 and 2, with the larger footprint locations showing a high degree of overlap with the sources (indicated by the red boxes). The enhancement observed at the 25.3-25.4° position may be influenced by sources located north of the study area.

In your second review comment, you noted that panels c and d are too small to view the colored DQ-1 XCO2 data, only showing the track. The original DQ-1 track data was too dense to clearly display the colored data, so we replaced it with pseudo-data tracks. We have also added an explanation in the figure caption regarding the blue triangles, which represent satellite-observed XCO2 data not used in the background line calculations (as we consider these to reflect the impacts of fossil fuel emission enhancements).

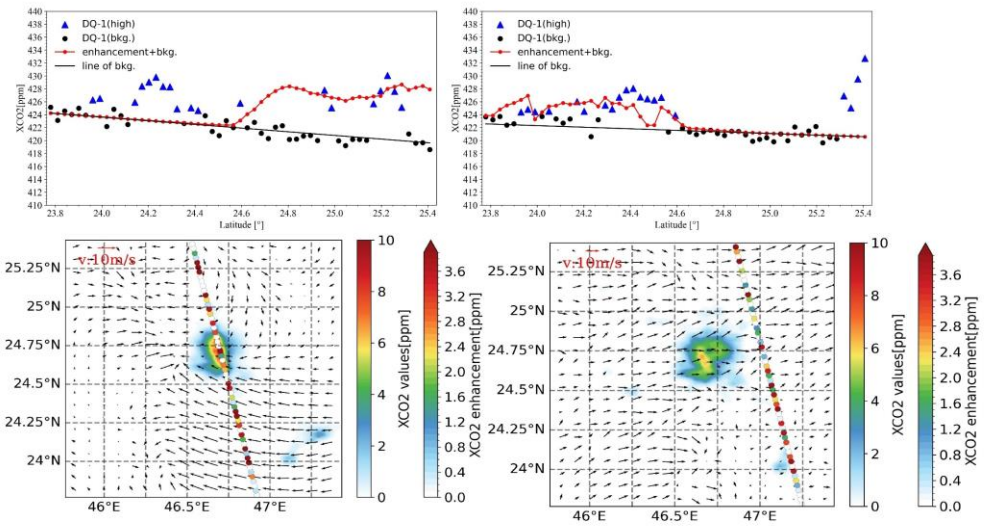

Figure S7. Figure 3 in the manuscript after modification

3.Figure 4: Please add the column averaged footprint figures (like fig 2c) to clarify the complex wind situations. The wind arrows are to small. All color bars seem wrong: the enhancements in the left line plots are much higher than in the right color plots.

ANSWER: Thank you very much for your suggestions regarding the revisions to Figure 4 in the manuscript. You requested the addition of a column-averaged footprint map similar to that in Figure 2c to clarify the complex wind conditions. Given that Figure 4 presents multiple tracks, we will focus on showcasing the two tracks passing over Cairo on August 2, 2022, and November 15, 2022 (represented as Figures S8 and S9, respectively).

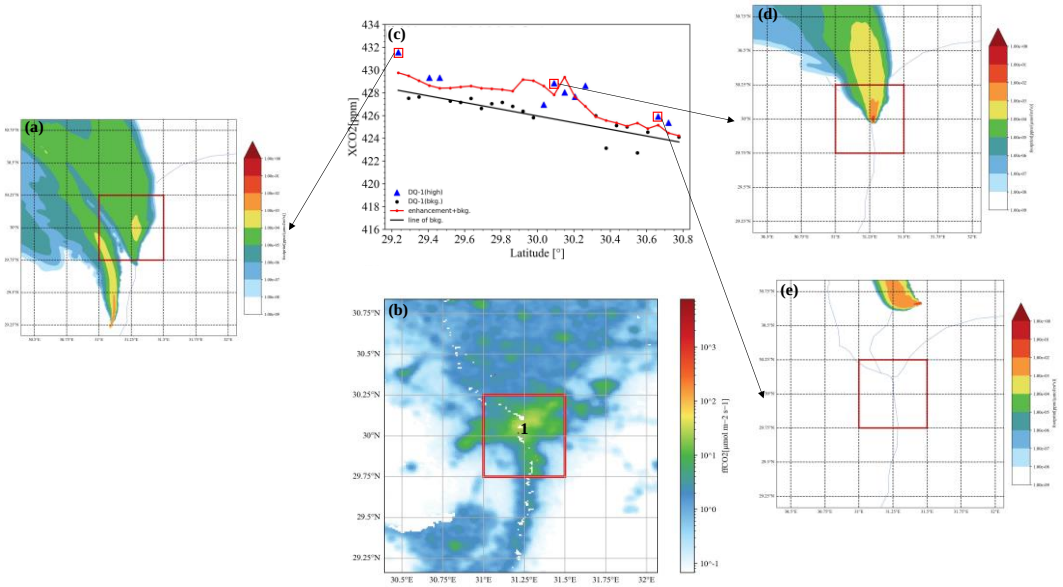

Figure S8. Similar to Figures S5 and S6, XSTILT and enhancement sources are shown for the XCO2 enhancement position of a portion of the DQ-1 orbit transiting Cairo on 15 November 2022 under complex wind conditions

Similar to Figures S5 and S6, Figure S8 presents the column-weighted footprint (X-footprint) simulating fossil fuel emissions and some DQ-1 pseudo-data point locations during the DQ-1 overpass of Cairo. From Figure S8, it can be observed that the simulated XCO2 enhancements within the ranges of 29.2-29.4° and 29.8-30.2° are primarily driven by the main urban emission source 1 (indicated by the red box). The enhancements in the 30.6-30.8° range are attributed to fossil fuel emissions from the northern part of the study area and possibly from sources located just outside the northern boundary of the study region.

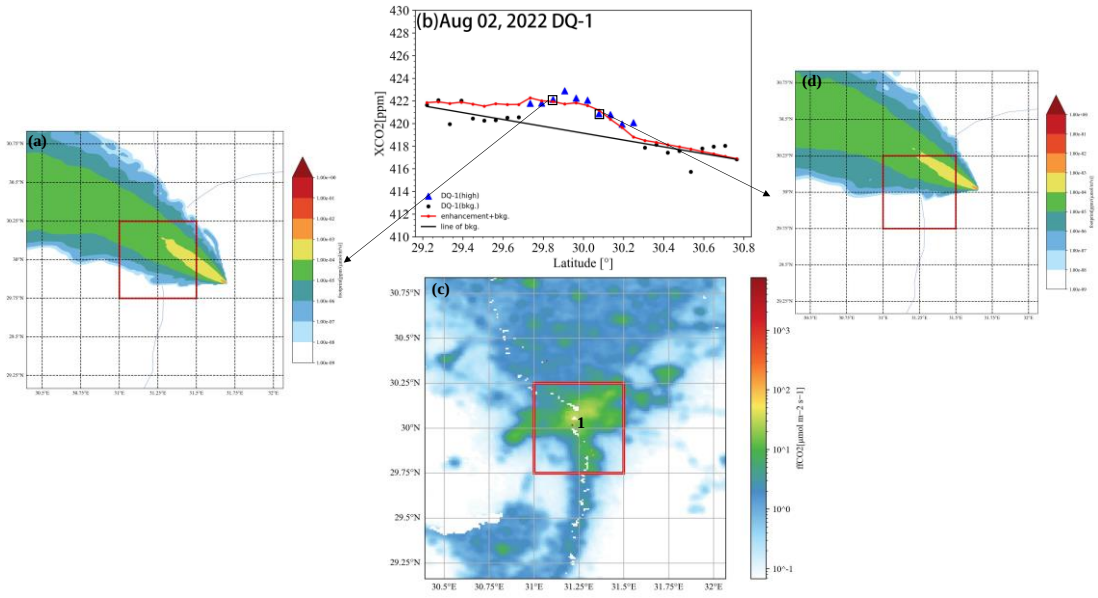

Figure S9. Similar to Figures S5 and S6, XSTILT and enhancement sources are shown for the XCO2 enhancement position of a portion of the DQ-1 orbit transiting Cairo on 02 August 2022 for complex wind conditions

Figure S9 is similar to Figure S8 and clearly demonstrates the impact of the main emission sources in the study area on the XCO2 enhancements observed by DQ-1 and those simulated by the high-resolution atmospheric transport model. Panels a and b indicate that the simulated enhancements in the range of 29.8-30.2° primarily originate from source 1 (red box 1).

You also mentioned that the wind arrows are too small and that there seems to be an error with the color bars: the enhancement values in the left line plot are significantly higher than those in the right colored map. We will enlarge the wind arrows in the revised manuscript. Regarding the color bar issue, we initially aimed for simplicity by combining the simulated plume (colored shading) and the track XCO2 enhancements into a single color bar. However, since the observed XCO2 enhancement range exceeds that of the simulated plume, it resulted in the discrepancy you noticed. In the revised manuscript, we will create two separate color bars for these components to resolve this issue. Thank you for your careful reading and for pointing out this problem.

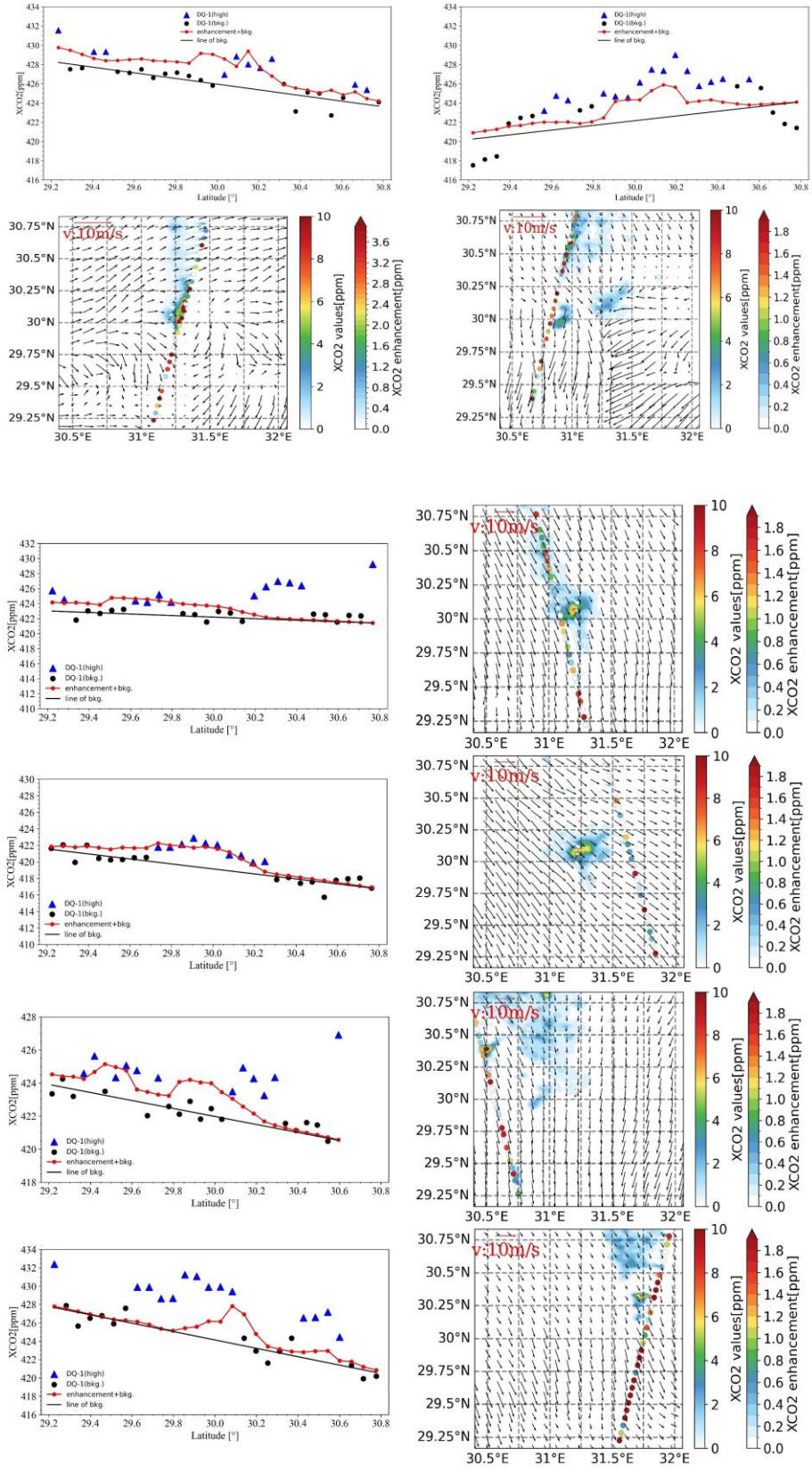

Figure S10. Figure 4 in the manuscript after modification

4.Figure 5: The DQ-1 orbit is not visible. The satellite image is too dark. Please mark the city center, the city limits and the TCCON site(s). The figure does not show the wind fields as stated in line 482.

ANSWER: Thank you very much for your suggestions regarding Figure 5. You pointed out that the DQ-1 track is not visible, and that the satellite imagery is too dark. We have modified the base map to clearly label the city center and urban boundaries, and we have marked the location of the TCCON station with a red pentagram.

You also noted that the wind field mentioned in line 482 was not displayed. We apologize for the confusion; the wind field referenced is related to line 481, where "The figure" refers to Figure 6, not Figure 5. Consequently, the references to Figure 5e-h in line 485 should be changed to Figure 6. Thank you for your careful reading, which helped us identify these oversights.

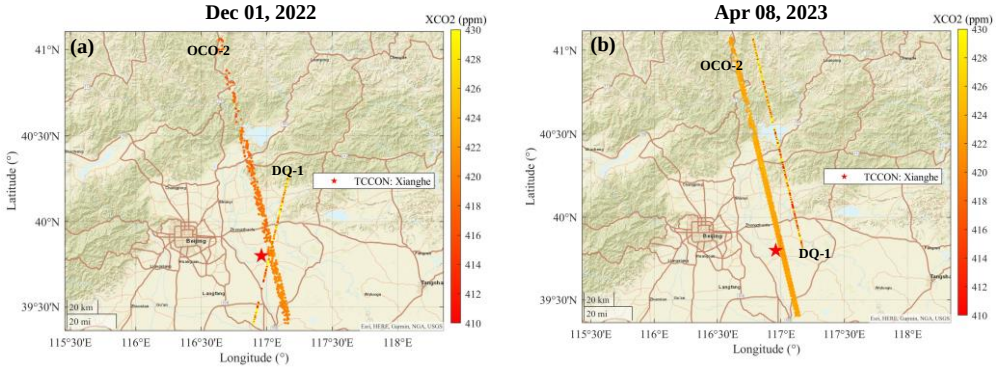

Figure S11. Figure 5 in the manuscript after modification

5.Section 3.3 Estimating Biosphere Fluxes: your statements concerning the natural emissions are based on the examination of very few cases, and thus need to be re-formulated more cautiously. For example, in line 582, only in figure 9d do the simulated enhancements align more closely with the observations, not in the other panels a, b, c. And in line 585, only figure 2c shows that the CASA and ODIAC enhancements differ significantly. Please re-formulate accordingly.

ANSWER: Thank you very much for your suggestions regarding Section 3.3. You pointed out that the statements about natural emissions are based on only a few cases and need to be rephrased more cautiously. For example, in line 582, it should be clarified that only the enhancement simulated in Figure 9d is more consistent with the observational results, while this is not the case for panels a, b, and c. In line 585, we should specify that only Figure 2c shows a significant difference in enhancements between CASA and ODIAC.

We will revise this section to reflect our findings more accurately regarding the use of diurnal orbits to study the impacts of natural emissions on the inversions. Thank you for your guidance!

6.References: in about half of all references the journal name is missing and the last author is misspelled. Eldering 2017, Han 2017, Miller 2014, and Wang 2014 are listed twice. In the manuscript, all citations should list only the first author and the year of publication.

ANSWER: Thank you very much for bringing up the errors that appeared in the references, we will check the references one by one in subsequent submissions of the revised manuscript to ensure that each reference meets the requirements of the journal.

Recommended minor changes:

1. line 23: The results of a case study indicate...

ANSWER: Revised

2. l 47: budget of the three fluxes: what do you mean? be more precise

ANSWER:

I sincerely thank the reviewers for suggesting a revision to this oversight in the manuscript. Once these background emissions are specified in space and time, the fluxes that are estimated in the inversion process, the "residual" fluxes, represent adjustments to the background fluxes such that the resulting CO2 concentration best matches atmospheric CO2 concentrations observed at particular times and locations. This may be expressed as(Gurney et al., 2005):

$$C_{obs} = C_{ff} + C_{oc} + C_{nbio} + \sum_{i=1}^{N} C_{res}$$

The three fluxes mentioned in line 47 represent C_{ff}, C_{oc} and C_{nbio}.

where C_{obs} represents observed CO2 at a particular points in space and time, C_{ff} represents the contribution to the observed CO2 due to global fossil fuel emissions, C_{oc}, the contribution due to a chosen global oceanic flux, C_{nbio}, the contribution due to a neutral biosphere flux, and C_{res}, the contribution of the residual fluxes from the chosen N discretized regions(Gurney et al., 2000).

We have replaced 'three fluxes' with 'global fossil fuel emission fluxes, choosing global oceanic flux and neutral biosphere flux' in lines 47-48.

3. l 49: ...emissions are located.

ANSWER: Revised

4. l 54 greenhouse gas measurements

ANSWER: Revised

5. l 85 which is onboard

ANSWER: Revised

6. l 92 a predetermined conclusion

ANSWER: We will remove the pre-determined conclusions you mentioned

7. l 99 used this tool

ANSWER: Revised

8. l 112 fine-scale trace gas transport

ANSWER: Revised

9. l 139 mention the LTAN (local time of ascending node) of DQ-1 to inform on the day/night capacity

ANSWER: DQ-1, as a sun-synchronous orbiting satellite, has a stable daily transit time of approximately 1 p.m. local time during the day and 1 a.m. local time at night

10. l 158 integrated weighting function

ANSWER: Revised

11. l 189 Atmospheric Model Setting

ANSWER: Revised

12. l 228 of the ACDL product.

ANSWER: Revised

13. l 277 described in equations 1 and 2.

ANSWER: Revised

14. l 287 the number of dry-air molecules per unit volume

ANSWER: Revised

15. l 290 change the XCO2(p) term in the integral on the right side of eq 3 into CO2(p)

ANSWER: Revised

16. figure 2: the legends are too small

ANSWER: Revised

17. l 330 and 394: a LEO orbit has a velocity of ~7 km/s, so either you averaged over 7 km, or over 0.5 sec

ANSWER: Line 394 mentions that our pseudo-data was obtained by averaging all the data in one second

18. l 387 nighttime observations can also be affected by aerosol and clouds, so explain better what

you want to state here

ANSWER: Here is a mistake in our expression, we mean that DQ-1 is different from other passive remote sensing satellites in that it is not only capable of night observation, but also less affected by clouds and aerosols. We'll revise this part of the description in the manuscript

19. l 399 Here, sigma represents the random error...

ANSWER: Revised

20. l 412 I guess the background XCO2 level is determined by the lidar? Please be more precise.

ANSWER: Here it is a case of sloppy presentation on our part, where background XCO2 level refers to the XCO2 background line derived in Section 2.3.3. Since the derivation of ffXCO2 relies on the observed XCO2 minus the background XCO2, the derivation of ffXCO2 is closely related to the establishment of the background XCO2.

21. l 485 Figures 6e-h ...

ANSWER: Revised

22. l 648 show these averages in table 1

ANSWER:

Table 1 Results of inversion of urban emission scaling factors for selected cities using DQ-1 XCO2 data

City	Overpass	Prior total emission (Mt C/month)	Prior total emission uncertainty (σ_a)	Measurement uncertainty ($\sigma_{measurements}$, units: ppm)	Transport model uncertainty (σ_{Model}, units: ppm)	Scaling factor(λ) ± posterior uncertainty（$\hat{\sigma}$）	OCO-2 Scaling factor/City mean factor
Riyadh	02 March 2023	2.37	45%	1.03	2.53	0.75±0.20	*0.80±0.18*
	20 June 2022	3.49		0.98	2.58	0.86±0.16	
Beijing	01 December 2022	4.61	25%	1.88/**2.11**	2.64	0.98±0.15	**1.09±0.18**
	08 April 2023	3.35		1.57/**1.93**	1.79	0.65±0.11	**0.70±0.14**
	09 January 2023	2.40		2.01	3.04	0.91±0.12	*0.83±0.13*
	10 January 2023	2.40		1.99	1.45	1.00±0.14	
	19 June 2022	3.81		1.78	2.11	0.96±0.16	
	20 June 2022	3.81		1.52	1.12	0.53±0.11	
Cairo	26 June 2022	2.43	45%	1.08	0.56	1.06±0.20	*1.10±0.14*

02 August 2022	2.49	1.45	0.71	0.98±0.12
16 August 2022	2.49	1.67	0.87	1.21±0.14
08 November 2022	1.96	1.22	0.36	1.15±0.16
15 November 2022	1.96	0.98	1.31	1.19±0.11
22 November 2022	1.96	1.11	0.21	1.06±0.13

Notes. Scaling factors and their a posteriori uncertainties are shown for each orbit, as well as integrated information for all selected orbits. Uncertainty components are listed for each track, including the a priori uncertainty in the scaling factor and the measurement and transport uncertainty in the integral ffXCO2 (some specific track data inverted using OCO-2 data are bolded, and the average emission scaling factor and a posteriori uncertainty for all tracks in each city are in the last column and highlighted in italics).

23. l 663 45%

ANSWER: Revised

24. l 744 June 2022 to April 2023

ANSWER: Revised

References

Alessio, S. M., Alessio, S. M. J. D. s. p., concepts, s. a. f. s., and applications: Discrete wavelet transform (DWT), 645-714, 2016.

Gurney, K., Law, R., Rayner, P., and Denning, S.: Transcom 3 experimental protocol, 2000.

Gurney, K. R., Chen, Y. H., Maki, T., Kawa, S. R., Andrews, A., and Zhu, Z. J. J. o. G. R. A.: Sensitivity of atmospheric CO2 inversions to seasonal and interannual variations in fossil fuel emissions, 110, 2005.

Lang, M., Guo, H., Odegard, J. E., Burrus, C. S., and Wells Jr, R. O.: Nonlinear processing of a shift-invariant discrete wavelet transform (DWT) for noise reduction, Wavelet Applications II, 640-651,

Ye, X., Lauvaux, T., Kort, E. A., Oda, T., Feng, S., Lin, J. C., Yang, E. G., and Wu, D. J. J. o. G. R. A.: Constraining fossil fuel CO2 emissions from urban area using OCO-2 observations of total column CO2, 125, e2019JD030528, 2020.